Structural phase transition and failure of nanographite sheets under high pressure: a molecular dynamics study

2007 J. Phys.: Condens. Matter 19 346224

(http://iopscience.iop.org/0953-8984/19/34/346224)

IOP PUBLISHING JOURNAL OF PHYSICS: CONDENSED MATTER

J. Phys.: Condens. Matter **19** (2007) 346224 (7pp) doi:10.1088/0953-8984/19/34/346224

Structural phase transition and failure of nanographite sheets under high pressure: a molecular dynamics study

Bin Zhang[1], **Yongcheng Liang**[1,2] **and Huiyu Sun**[1]

[1] College of Aerospace Engineering, Nanjing University of Aeronautics and Astronautics, Nanjing 210016, People's Republic of China
[2] College of Engineering Science and Technology, Shanghai Fisheries University, Shanghai 200090, People's Republic of China

E-mail: beenchang@nuaa.edu.cn

Received 23 March 2007, in final form 28 June 2007
Published 26 July 2007
Online at stacks.iop.org/JPhysCM/19/346224

Abstract

Nanographite sheets under high compressive stresses at ambient temperature have been investigated through molecular dynamics simulations using the Tersoff–Brenner potential. Nanographite undergoes a soft to hard phase transition at a certain compressive stress, about 15 GPa. With increasing compressions, the bonding structures of nanographite are changed, interlayer sp^3-bonds are formed, and nanographite transforms into a superhard carbon phase (SCP). Further compressions lead to the instabilities of the SCP. Although the detailed lattice structure of the SCP remains elusive, its compressive strength can approach 150 GPa, comparable to that of diamond. The maximum failure stresses of nanographite sheets are sensitive to the inter-and intra-layer interstices. Our results may explain paradoxical experimental results in the available literature.

(Some figures in this article are in colour only in the electronic version)

1. Introduction

Carbon can exist in diverse forms, such as carbynes, graphite, nanotubes, fullerenes and diamond, because of its capability to form various interatomic bonding structures. Graphite is soft in a layered structure of hexagonal carbon rings with sp^2-bonding, and cubic diamond is the hardest natural mineral in a tetrahedral structure with sp^3-bonding. As a monolayer of graphite, graphene exhibits an exceptionally high crystal and electronic quality and is an extremely promising material for materials science and condensed-matter physics [1, 2]. However, graphite and diamond can be transformed from one to the other at high pressures and

elevated temperatures, and the pressure-induced transformation path has been proposed by *ab initio* molecular dynamics (MD) simulations [3].

Under high-pressure conditions, some materials undergo phase transitions and show novel physical and mechanical properties, such as superhardness, high yield strength, magnetism and superconductivity. These fascinating physical behaviors have captured the interest of scientists. Diamond anvil cells can attain a static pressure of more than 400 GPa, and are widely used to develop new materials for technological applications [4]. A structural phase transition to a tetrahedral diamond phase in graphite beginning at 15 GPa was completed at 55 GPa and *did not* produce a superhard carbon phase (SCP) until 65 GPa [5] under nonhydrostatic pressure. However, when the diamond culets came into contact with a fine polycrystalline aggregate of graphite in diamond anvil cells, the graphite became hard enough to crack diamond under extreme high nonhydrostatic pressure [6]. On the other hand, diamond at the point of indentation transformed into disordered graphite slightly below 100 GPa [7]. Why can soft graphite crack diamond? There is a paradox in these experimental phenomena. Furthermore, a SCP could be also synthesized by cold compression of carbon nanotubes at about 75 GPa [8].

Our theoretical predictions [9, 10] and the above experimental results [5–8] imply that there may be a *new* superhard phase between graphite and diamond. These predictions have been verified by an intermediate carbon phase [11] and a novel crystalline polymorph of carbon resulting from a natural shockwave event [12]. An intermediate carbon phase between diamond and graphite was found following neutron irradiation of natural diamond [11]. A *new* hard transparent carbon phase (not hexagonal diamond) was found in a rock sample from the Popigai impact crater in Russia [12]. In a recent attempt to identify this *new* phase, some hypothetical superhard structures of carbon, honeycomb structures, C_6-bcc and C_{20}-sc cubic structures, were proposed [13, 14]. But predominantly a *ta-C* amorphous carbon with ordered sp^3 clusters was formed by rapid quenching of liquid carbon [15]. Consequently, it is interesting to conduct theoretical calculations to predict the formation, structure and strength of the new SCP which remains a paradox.

Here we report MD simulations on the phase transition, bonding structures and theoretical strengths of nanographite sheets under ultrahigh compressive stresses at room temperature.

2. Molecular dynamics simulations and results

2.1. Models

In our MD models in figure 1(a), graphene sheets are AB-stacked in a cuboid and the lattice parameters of graphite are $a = 2.46$ Å and $c = 6.80$ Å with $c/a = 2.76$. Carbon atoms are arranged in a graphite cuboid of 2.84 nm in length and 3.08 nm in width. The bottom layer is completely fixed, and the top layer serves as a displacement loading plate by which uniform displacements in the $-z$ direction are applied quasi-statically to the bottom sheet with an average velocity of 0.05 Å ps^{-1} (5.0 m s^{-1}). We design cuboid models containing five effective layers of graphene sheets with different interplanar interstices Δ_x and Δ_y to consider the influences of interlayer sliding (see figure 1(b)), where Δ_x and Δ_y are the maximum possible interplanar shear deformations. Therefore the effective layers of graphene sheets are similarly placed between two infinite in-plane-fixed graphene sheets when periodic boundary conditions (PBC) are applied to the MD models. When $\Delta_x/l_{x0} = 0$ and $\Delta_y/l_{y0} = 0$, the models represent infinite perfect films. When $\Delta_x/l_{x0} > 0$ and $\Delta_y/l_{y0} > 0$, the models represent infinite films containing interstices. Under uniform compressions in the z direction, quasi-hydrostatic stress states (with little shear deformation) will be obtained in the models without interplanar interstices (case I in figure 2), while nonhydrostatic stress states will be

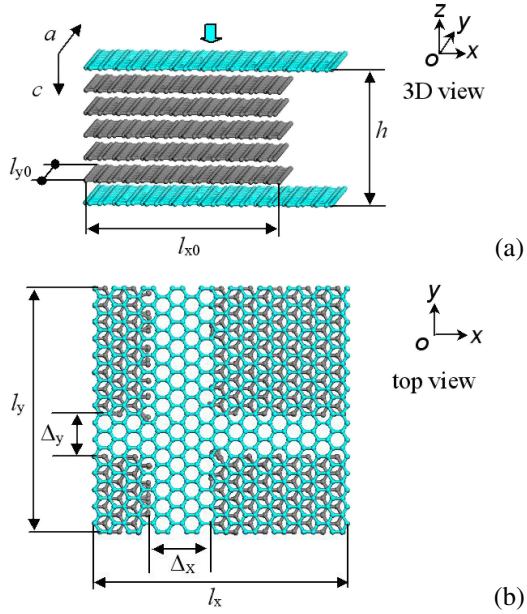

Figure 1. Molecular dynamics simulation models of nanographite sheets with five effective graphene layers (gray). (a) Original model. The bottom cyan graphite layer is fixed, the top cyan one serves as a loading plane in the $-z$ direction, and the height $h = 2.04$ nm. l_{x0} and l_{y0} are the width and length of the film, respectively. (b) The model after applied periodic boundary conditions. l_x and l_y are the width and length of the periodic box, respectively. Δ_x $(= l_x - l_{x0})$ and Δ_y $(= l_y - l_{y0})$ are introduced to model the interplanar interstices.

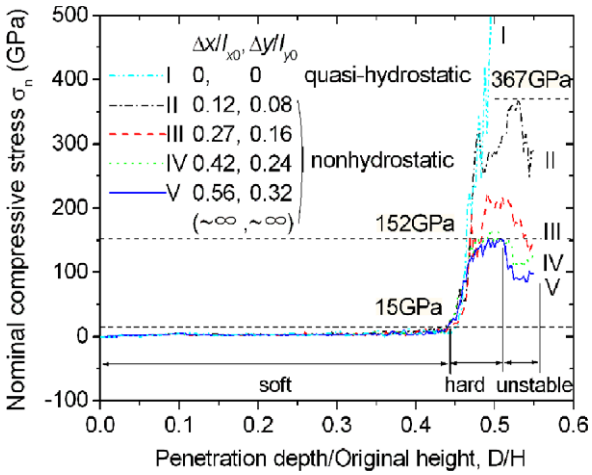

Figure 2. Nominal compressive stress σ_n versus strain D/H (the ratio of penetration depth D to original height H) curves of the nanographite sheets. When $\Delta_x/l_{x0} = 0$ and $\Delta_y/l_{y0} = 0$, quasi-hydrostatic stress states are generated (case I); when $\Delta_x/l_{x0} > 0$ and $\Delta_y/l_{y0} > 0$, nonhydrostatic stress states are generated (cases II–V).

obtained in the models containing interplanar interstices (cases II–V in figure 2 where Δ_x and Δ_y are one to four times the height and width of a hexagonal carbon ring, respectively).

2.2. Empirical interatomic potential used in the simulations

By use of the Tersoff potential, nanoindentation simulations can be used to obtain elastic moduli of graphite and diamond, which are in good agreement with experimental results [16]. The second-generation Tersoff–Brenner potential is a well developed reactive bond order potential for carbon-related solids, which itself is carefully and specifically developed on the basis of the Tersoff potential and fitted with reference to a large experimental and density functional database of many important parameters of carbon. Systematic comparisons of the predicted bond length, energies and force constants with the experimental and density functional results show that the potential is more reliable than the well-known Tersoff potential, yielding results that can be compared reasonably well with predictions from the first-principles calculations for diamond [17]. The potential has been modified to describe the interatomic interaction of carbon atoms in diamond and graphite lattices, and nonlocal effects have also been incorporated via an analytic function. The capability of the potential to correctly describe the bond breaking and switching among multi-carbon atoms has been verified [18, 19], and the nonbonding interatomic interaction in the form of a Lennard-Jones 6–12 potential [20] has also been included.

In our MD simulations, the second-generation Tersoff–Brenner potential is used. The present molecular system is coupled to a heat bath of the Berendsen scheme [21] for a constant temperature (300 K) simulation (NVT ensemble), and the time step is set to 0.5 fs and the period for equilibration is 1.0 ps for sufficient accuracy.

2.3. Analyses of the MD simulation results

Under high pressures, the curves of nominal compressive stress σ_{n} versus strain (the ratio of penetration depth D to original height H, D/H) for the nanographite sheets are presented in figure 2, where σ_{n} is defined as the z-direction (figure 1(a)) resultant force of the atoms in the top plane divided by the contact area between the displacement loading plate and the effective nanographite sheets. We count all the atoms which support the z-direction nonzero force f_i in the loading plane, and get a total number n; then the resultant force $F = \sum_{i=1}^{n} f_i$. If each atom occupies half the area of a standard hexangular carbon ring, $s_i = \sqrt{3}/4a^2$ ($a = 2.46$ Å), the total contact area $S = \sum_{i=1}^{n} s_i$. Therefore, $\sigma_{\mathrm{n}} = F/S$.

Under nonhydrostatic pressure, there are three typical regions in the nominal compressive stress–strain curves of the nanographite sheets: soft, hard and unstable regions (figure 2(II–V)). In the soft phase region where the average interlayer distance h_0 ranges from 3.4 to 1.9 Å, σ_{n} is low and increases slowly with D/H up to about 15 GPa, beyond which phase transition would occur, but no interlayer sp^3-bonding is formed. In the hard phase region where h_0 ranges from 1.9 to 1.7 Å, σ_{n} increases sharply but still linearly when h_0 is greater than 1.8 Å, and interlayer sp^3-bonding seldom occurs. The average slopes of the curves (namely the elastic moduli) in the hard phase region are hundreds of times higher than those in the soft phase region. When h_0 is less than 1.8 Å, large numbers of interlayer sp^3-bonds similar to the hard ones in diamond are formed and increase monotonically, while σ_{n} increases nonlinearly. In the unstable region where h_0 is less than 1.7 Å, more and more interlayer sp^3-bonds formed, but σ_{n} drops due to the interlayer shear deformation. The formed sp^3-bonds will break when h_0 is less than 1.57 Å, and the structure of the hard-phase graphite becomes unstable.

We have carefully examined the MD simulation results in figure 2(II–V) and found that the soft to hard phase-transition region corresponds to approximately $h_0 = 1.9$–1.8 Å. With further compressions, the limiting failure stress decreases from 367 to 152 GPa with the interstices Δ_x/l_{x0} increasing from 0.12 to 0.56 and Δ_y/l_{y0} from 0.08 to 0.12. Interlayer shear deformations occur during the compressions, and some graphene sheets become disordered and

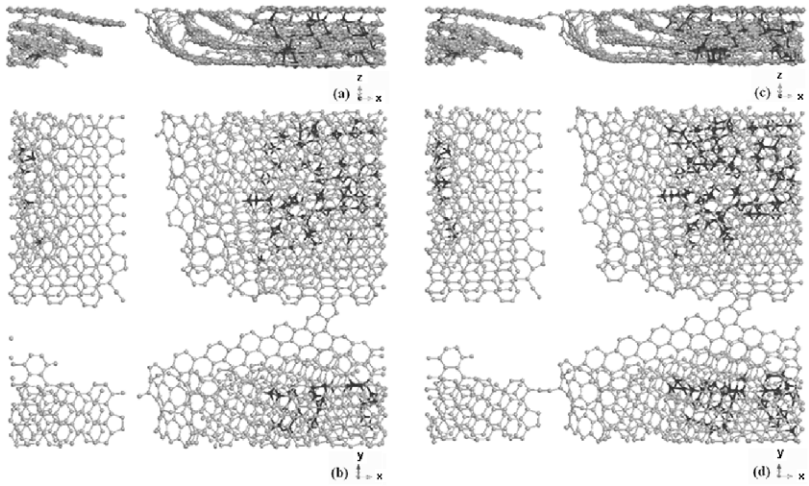

Figure 3. Bonding structure and shear deformation of the compressed nanographite sheets in figure 2(V) when $D/H = 0.49$ and $\sigma_n = 152$ GPa for (a)/(b), $D/H = 0.51$ and $\sigma_n = 152$ GPa for (c)/(d): (a) and (c) are front views; (b) and (d) are top views. Interlayer sp^3-bonding atoms (dark grey/red) fractions are 6.54% in (a)/(b) and 8.85% in (c)/(d).

buckling and interlayer covalent bonds are formed near the free edges. As the atom number in our MD models increases with Δ_x and Δy and the calculation time increases sharply with the atom number, we chose $\Delta_x/l_{x0} = 0.56$ and $\Delta_y/l_{y0} = 0.32$ to approach $\Delta x = \sim\infty$ and $\Delta y = \sim\infty$ in figure 2(V). This yields the similar results to larger Δ_x/l_{x0} and Δ_y/l_{y0} for the in-plane constraints of interlayer covalent bonds near the free edges. The evolution of sp^3-bonding structures at $\sigma_n = 152$ GPa of case V in figure 2 is shown in figures 3(a)–(d). σ_n reaches 152 GPa first at $D/H = 0.49$ where 6.54% of the atoms formed interlayer sp^3-bonds, and then drops. But interlayer sp^3-bonding atoms increased with D/H, and σ_n reaches 152 GPa again at $D/H = 0.51$ where 8.85% of the atoms formed interlayer sp^3-bonds. After σ_n reaches 152 GPa twice, the hard phase fails. The activation energy barrier, which prevents the sliding of graphene sheets and the formation of interlayer sp^3-bonding, also depends on the scale of the atoms in our models. Maybe the high mobility between different stacking graphite and a large amount of interlayer sp^3-bonding observed in [3] is due to a smaller number of atoms employed in their models. Therefore, the compressive strength of nanographite can approach 152 GPa, which is comparable to the reversible structure-transition pressure of diamond [22] and is higher than either the nominal compressive strength [7] or the calculated shear strength of diamond [23, 24].

The above theoretical compressive strength of nanographite is certainly associated with the boundary constraints and loading configurations, which can influence stress states. The hydrostatic part of the stress tensor reduces the bond lengths, and the nonhydrostatic (deviator) part changes the bond angles, which is essential for the transformations between graphite and diamond [25]. Shear stress has often been shown to be a prime factor in the high-pressure behaviors of solids. We show here the effect of the possible shear stress. In the absence of shear stresses, the number of formed sp^3-bonds increases monotonically. However, the formed sp^3 bonds will break in the nonhydrostatic case beyond the limited compressive stress due to the shear deformation. Small shear deformation will significantly reduce the threshold compressive stress of sp^3-bond formation. The interlayer sp^3-bonding mainly occurred between the bridging carbon atoms which pair with atoms in an adjacent layer. The interstices between the

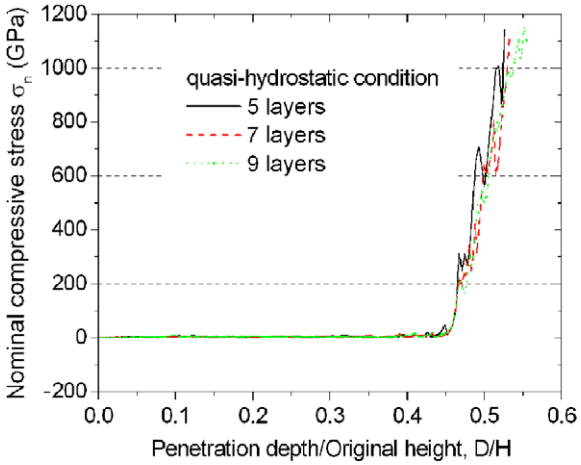

Figure 4. Nominal compressive stress (σ_n) versus strain (D/H) curves of nanographite sheets (containing five, seven or nine layers) under ultrahigh quasi-hydrostatic pressures.

nanographite is related to its sizes and stress states, since well ground polycrystalline graphite could quickly develop a preferred ordination with the c-axis parallel to the loading direction under compression [6]. The interstices would become small, and the nanographite would be merged into a larger film in quasi-hydrostatic conditions. In the larger graphite film, the atoms at the edges can easily form bonds, which constrain the graphene layers to slip out. The stress states become similar to hydrostatic conditions, and phase transition is difficult. Thus only nanographite could undergo structural phase transition easily in the experiment [6].

MD simulations are also performed on graphite models containing five and nine layers without interstices under PBC, which represent infinite perfect graphite films under quasi-hydrostatic pressure (figure 4), similar to the case I in figure 2. All the simulations we have performed confirm that the soft to hard phase transition always occurs at about 15 GPa, independent of the number of layers as well as the boundary conditions, which is consistent with the experimental results [5, 6]. The mean interlayer distance h_0 is about 1.87 Å when the soft to hard phase transition occurs, which is smaller than that for nanographite in nonhydrostatic states. The compressive stresses in quasi-hydrostatic states, where few shear stresses occur, increase smoothly before the first drop occurs. The curves are nearly independent of the number of graphite layers within 200 GPa, and the general trends stay the same in the whole simulation range except the discontinuous drops beyond 200 GPa. The interlayer sp^3-bonding did not form until σ_n reached about 600 GPa, which shows a high activation energy barrier. The number of sp^3-bonds formed increases monotonically, and the structure is difficult to destroy, even with stresses up to 1.0 TPa.

In this paper, we are mainly concerned with the phase transition and compressive strength of hard-phase graphite, though the bulk properties of both graphite and diamond under ultrahigh pressure are rich and colorful, such as hardness, toughness and abrasion resistance. Some new phase of carbon under high pressure is still unclear, and further work is ongoing.

3. Conclusions

Under ultrahigh cold compressions, nanographite sheets will undergo soft to hard structural phase transitions at about 15 GPa. The nominal compressive stresses of the hard carbon phase are sensitive to the interlayer shear deformation, and the compressive strength is about 150 GPa,

which is even higher than the strength of diamond. Our results indicate that a *new*, *superhard* phase containing sp^3-bonds may exist during the compression of nanographite, but there is no evidence to show that its crystal lattice structure is either diamond or another available carbon form.

Acknowledgments

The authors acknowledge the NSF of China (no. 10602023), the NSF of Jiangsu Province of China (no. BK2007190) and the Research Startup Fund of Nanjing University of Aeronautics and Astronautics.

References

[1] Geim A K and Novoselov K S 2007 *Nat. Mater.* **6** 183
[2] Harigaya K 2001 *J. Phys.: Condens. Matter* **13** 1295
[3] Scandolo S, Bernasconi M, Chiarotti G L, Focher P and Tosatti E 1995 *Phys. Rev. Lett.* **74** 4015
[4] Mcmillan P F 2002 *Nat. Mater.* **1** 19
[5] Patterson J R, Kudryavtsev A and Vohra Y K 2002 *Appl. Phys. Lett.* **81** 2073
[6] Mao W L *et al* 2003 *Science* **302** 425
[7] Gogotsi Y G, Kailer A and Nickel K G 1999 *Nature* **401** 663
[8] Wang Z *et al* 2004 *Proc. Natl Acad. Sci.* **101** 13699
[9] Zhang B and Guo W 2005 *Appl. Phys. Lett.* **87** 051907
[10] Guo W, Zhu C Z, Yu T X, Woo C H, Zhang B and Dai Y T 2004 *Phys. Rev. Lett.* **93** 245502
[11] Blank V D *et al* 1999 *Diamond Relat. Mater.* **8** 1285
[12] Goresy A El, Dubrovinsky L S, Gillet P, Mostefaoui S, Graup G, Drakopoulos M, Simionovici A S, Swamy V and Masaitis V 2003 *C. R. Geosci.* **335** 889
[13] Ribeiro F J, Tangney P, Louie S G and Cohen M L 2006 *Phys. Rev.* B **74** 172101
[14] Ribeiro F J, Tangney P, Louie S G and Cohen M L 2005 *Phys. Rev.* B **72** 214109
[15] Sorkin A, Adler J and Kalish R 2006 *Phys. Rev.* B **74** 064115
[16] Richter A, Ries R, Smith R, Henkel M and Wolf B 2000 *Diamond Relat. Mater.* **9** 170
[17] Brenner D W, Shenderova O A, Harrison J A, Stuart S J, Ni B and Sinnott S B 2002 *J. Phys.: Condens. Matter* **14** 783
[18] Yakobson B I, Brabec C J and Bernholc J 1996 *Phys. Rev. Lett.* **76** 2511
[19] Harrison J A, White C T, Colton R J and Brenner D W 1992 *Surf. Sci.* **271** 57
[20] Nardelli M B, Yakobson B I and Bernholc J 1998 *Phys. Rev.* B **57** R4277
[21] Berendsen H J C, Postma J P M, van Gunsteren W, DiNola A and Haak J R 1984 *J. Chem. Phys.* **81** 3684
[22] Mao H K and Hemley R J 1991 *Nature* **351** 721
[23] Chacham H and Kleinman L 2000 *Phys. Rev. Lett.* **85** 4904
[24] Zhang Y, Sun H and Chen C 2005 *Phys. Rev. Lett.* **94** 145505
[25] Gilman J J 1993 *Science* **261** 1436